SCIENTIFIC REPORTS

OPEN

CONFERENCE PROCEEDINGS

APEnergy2014

SUBJECT AREAS:
ELECTROCHEMISTRY
ELECTRONIC MATERIALS

Received
23 December 2013

Accepted
20 January 2014

Published
29 August 2014

Correspondence and requests for materials should be addressed to C.B.C. (cbcao@bit.edu.cn)

Ultrathin Nickel Hydroxide and Oxide Nanosheets: Synthesis, Characterizations and Excellent Supercapacitor Performances

Youqi Zhu[1], Chuanbao Cao[1], Shi Tao[2], Wangsheng Chu[2], Ziyu Wu[2] & Yadong Li[3]

[1]Research Center of Materials Science, Beijing Institute of Technology, Beijing 100081, China, [2]National Synchrotron Radiation Laboratory, University of Science and Technology of China, Hefei 230029, China, [3]Department of Chemistry, Tsinghua University, Beijing 100084, China.

High-quality ultrathin two-dimensional nanosheets of α-$Ni(OH)_2$ are synthesized at large scale via microwave-assisted liquid-phase growth under low-temperature atmospheric conditions. After heat treatment, non-layered NiO nanosheets are obtained while maintaining their original frame structure. The well-defined and freestanding nanosheets exhibit a micron-sized planar area and ultrathin thickness (<2 nm), suggesting an ultrahigh surface atom ratio with unique surface and electronic structure. The ultrathin 2D nanostructure can make most atoms exposed outside with high activity thus facilitate the surface-dependent electrochemical reaction processes. The ultrathin α-$Ni(OH)_2$ and NiO nanosheets exhibit enhanced supercapacitor performances. Particularly, the α-$Ni(OH)_2$ nanosheets exhibit a maximum specific capacitance of 4172.5 F g^{-1} at a current density of 1 A g^{-1}. Even at higher rate of 16 A g^{-1}, the specific capacitance is still maintained at 2680 F g^{-1} with 98.5% retention after 2000 cycles. Even more important, we develop a facile and scalable method to produce high-quality ultrathin transition metal hydroxide and oxide nanosheets and make a possibility in commercial applications.

Because of high power density, fast charging time, and long lifespan, supercapacitors have recently received considerable attention for the increasing demand in advanced energy storage devices, especially with the emergence of electric vehicles. Pseudocapacitors, mainly employing the fast reversible multi-electron surface Faradaic redox reactions from electrode materials such as $Ni(OH)_2$[1,2], MnO_2[3], NiO[4–6], and Co_3O_4[7], often exhibit very high specific capacitance. However, pseudocapacitive charge storage sites are only limited on surface/near-surface, the bulk of materials cannot be used, causing very low active material utilization with non-competitive energy density to batteries. They also suffer from limited electrochemical stability under higher rates[2]. They cannot keep good rate capability and high reversibility, simultaneously, for their high dependence on Faradic redox reactions and in general unfavorable reaction kinetics under high rates. In this regard, the option is to explore novel pseudocapacitive materials, where high capacitance is still being retained at fast charge/discharge rates without any obvious capacity decay or leaving little portion of electrochemical active materials inactive under prolonged cycling, i.e., favorable reaction kinetics and high active material utilization are guaranteed.

Recently, the ultrathin two-dimensional (2D) nanomaterials, such as graphene and inorganic nanosheets, have attracted tremendous attention due to their fascinating physical and chemical properties for great potential applications in field-effect transistors, energy storage and conversion, topological insulators, and so on[8–11]. Generally, the ultrathin 2D nanomaterials are nearly made up of surfaces with molecular-scale thickness, causing a high percentage of surface atoms and high efficient active sites on the exposed surface. Consequently, the theoretical lithium storage capacity of graphene is improved to 744 mA h g^{-1}, two times as that of graphite, when both sides occupied by Li^+ to form LiC_3 structures[12]. The unique structure and surface properties of the ultrathin 2D nanomaterials make them more attractive in catalysis and energy devices[13–15]. More importantly, the ultrathin 2D nanostructures can provide short ion and electron diffusion path distances, large electrochemical active sites and electrode-electrolyte interface, high electronic conductivity, and improved structural stability[16]. So it can be concluded that the ultrathin 2D nanostructures are the most ideal morphological foundation for the surface-

dependent electrochemical reactions[17], representing a very interesting target with great promise for application in next generation batteries and supercapacitors[9,10,18].

However, the exfoliation of layered compounds and high-temperature epitaxial growth are the dominant ways to produce ultrathin 2D nanomaterials. The former is usually uncontrollable in the uniformity of size and shape, thickness, and lateral dimension; while the latter is highly dependent on growth substrates and/or noble metal catalysts accompanied with a low yield and high cost. It has been reported that solution-phase methods, such as solvothermal or colloidal growth reactions, can offer a facile production of 2D materials at gram scale quantities[19,20]. The recent successes in solution synthesis of PbS and CeO_2 ultrathin nanosheets show good promises in producing large quantities of 2D nanostructures[21,22], but their synthetic processes remain sophisticated and time-consuming. The facile and cost-efficient synthesis of high-quality ultrathin 2D nanomaterials, especially large-area non-layered nanosheets, at large scale has met with limited success and is still extremely urgent. Still, there exists the possibility to create single-atom or few-atom thick 2D layers from any material[23]. With respect to the exploration of various potential 2D nanomaterials, it is a great challenge to develop a universal strategy for fabricating those ultrathin 2D nanostructures.

Herein, we report a facile and scalable synthesis of high-quality ultrathin 2D nanosheets of lamellar hydroxides and non-layered metal oxides through microwave-assisted method. Based on the observed formation mechanism, we have successfully synthesized ultrathin Ni-based hydroxide and oxide nanosheets under mild experimental conditions. We also discover that the large-area ultrathin 2D nanostructures can significantly improve the surface-dependent electrochemical processes. In case of our ultrathin α-$Ni(OH)_2$ and NiO nanosheets, superior electrochemical activity for supercapacitors is achieved.

Results

The preparation process can be summarized in Figure 1a. The fundamental process is dependent on liquid-phase growth of ultrathin lamellar nickel hydroxide precursor under microwave irradiation. This stage undergoes a homogeneous alkalinization of nickel(II) nitrate solutions by urea hydrolysis through inductive effect of microwave irradiation under low-temperature atmospheric conditions. This process is conducted in a 1000 mL three-necked flask in microwave reactor (Figure S1a). The comfortable thermodynamic and kinetic factors are favorable for growth of ultrathin intermediate[24,25]. The formation of ultrathin nanosheets is dominated by a self-assembly and oriented attachment mechanism. The rapid microwave heating can facilitate the super saturation of reactant species, leading to the instantaneous formation of ultrafine nanocrystals and then spontaneous self-assembling or oriented attachment by intrinsic driving force of lamellar nickel hydroxide for 2D anisotropic growth. After heat treatment at 300°C (Figure S2a), α-$Ni(OH)_2$ nanosheets are completely decomposed into NiO. Figure S2b shows that single crystalline phase of α-$Ni(OH)_2$ with a hexagonal layered structure (JCPDS 22-0444) was obtained. All the diffraction peaks of NiO are consistent with a face-centered cubic phase (JCPDS 04-0835). The as-synthesized α-$Ni(OH)_2$ precursor exhibits a geometrically sheet-like 2D structure (Figure 1b). They are uniform and freestanding with a micron-sized planar area. The nanosheets are comprised of ultrafine nanocrystals arranging in planar direction (Figure S3). The sheet-like 2D morphology can be perfectly retained after heat treatment (Figure 1c), and there are no apparent broken or collapsed structures in the final sample, suggesting a good structural stability of this 2D structure. Figure 1d further reveals a highly flexible and gauze-like morphology of non-layered NiO.

Figure 2a further shows the freestanding and large-area sheet-like morphology of α-$Ni(OH)_2$, none of them assembles into a 3D hierarchical architecture. Figure 2b–c reveal their clear and well-defined outline with highly flexible and transparent features, suggesting fundamental characteristics in common of this kind of ultrathin sheet-like nanostructure. HRTEM investigation in the edge areas of ultrathin nanosheets is a common and direct method to determine the layer thickness microscopically[9]. Figure S4a collected from the folded edge or protuberant ridge of α-$Ni(OH)_2$ nanosheets demonstrates an average thickness of ~1.52 nm, suggesting that the nanosheets is comprised of 2–3 layers of octahedral $Ni(OH)_6$ arranging in hexagonal symmetry on planar direction. The XPS analysis is further carried out to determine the composition and the surface electronic state of the as-synthesized α-$Ni(OH)_2$ nanosheets (Figure S5). Only oxygen and nickel species are detected.

SAED pattern (inset in Figure 2c) indicates a polycrystalline nature of the overall NiO nanosheets. The three marked diffraction rings correspond to the {111}, {200}, and {220} planes, respectively. Figure 2d shows that the NiO nanosheet in the selected region shares the same lattice fringe and crystallographic orientation, indicating the same behavior in short range during the crystal transformation. Some observed small pores are irregularly distributed on surface causing a high roughness, which could be created by the evacuation of gaseous contents. FFT pattern (Figure 2e) collected from the area of regular lattice fringes reveals single-crystalline feature. Figure 2f shows some visible lattice fringes with an equal interplanar distance of 2.4 Å, corresponding to (111) planes of cubic NiO. Figure 2g demonstrates a ~1.16 nm layer thickness of NiO. As expected, the specific surface area of α-$Ni(OH)_2$ and NiO nanosheets is as high as 190.15 and 196.01 $m^2 g^{-1}$ (Figure S6). Such high values are associated with the unique structure of ultrathin nanosheets with extended and rough surfaces. More interestingly, it is found that the NiO

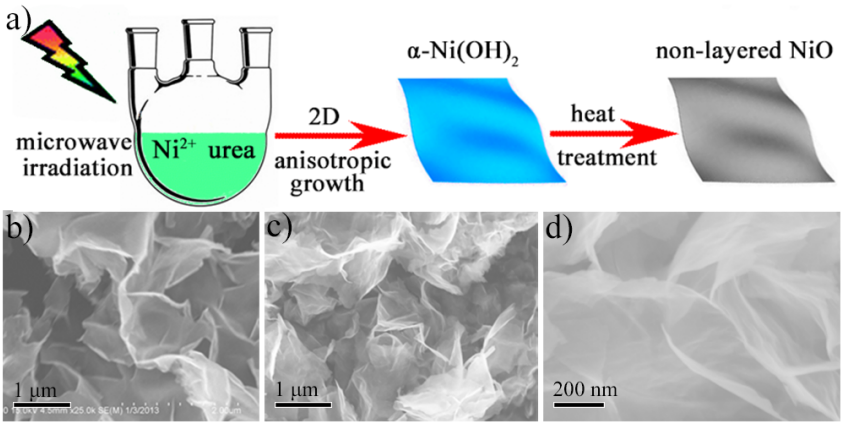

Figure 1 | (a) Schematic illustrating synthesis of nanosheets; FESEM images of (b) α-$Ni(OH)_2$ and (c), (d) NiO nanosheets.

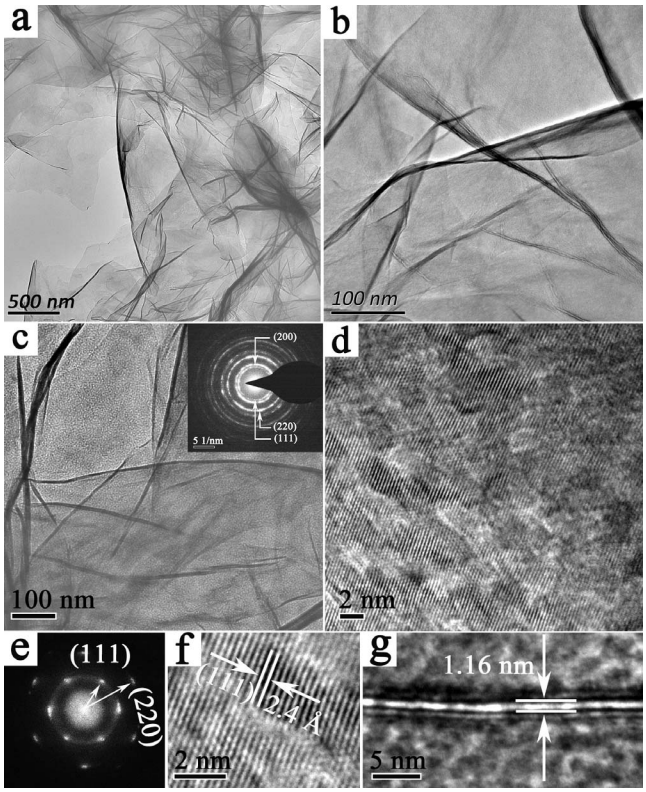

Figure 2 | (a) low and (b) high magnification FESEM images of α-$Ni(OH)_2$ nanosheets; (c) TEM image (the inset showing SAED pattern), (d) a planar HRTEM image, (e), (f) the corresponding FFT pattern and enlarged HRTEM image recorded from (d), and (g) a vertical HRTEM image of NiO nanosheets.

nanosheets can form a stable and uniform dispersion in ethanol for weeks (Figure S1d).

Compared with traditional wet-chemical syntheses, the microwave-assisted liquid-phase growth can decrease reaction time to less than 20 minutes[26]. The formation of precursor nanosheets is finished in a very short time. After 3 minutes under microwave irradiation with subsequent heat treatment, the perfect non-layered NiO nanosheets can be obtained (Figure S7a). Obviously different from the previously reported wet-chemical syntheses and the analogous microwave-activated procedure[22,26], the current reaction systems can avoid the morphology transformation to 3D hierarchical structures with prolonged reaction time. Figure S7a–d show that the non-layered NiO nanosheets synthesized with different microwave irradiating time (3, 5, 15, and 30 minutes) nearly exhibit the same morphology. It could be attributed to the fast local heating from microwave activation and the good structural stability of those nanosheets. This is the first report about a synthesis of freestanding low-dimensional nanostructures, especially ultrathin 2D nanosheets, that independent of reaction time.

In the experiments, it is found that the crucial reaction parameter is water. The formation of nanosheets strongly depends on the effects of the water molecules. Under the optimal amounts of water, the NiO samples exhibit a freestanding and large-area sheet-like morphology. Whereas with the contained water decreasing, the final products become folded and assemble into a flower-like quasi-spherical 3D hierarchical architecture (Figure S8a), although retaining their sheet-like building blocks (Figure S8b). In the absence of water, the final morphology further evolves into spherical aggregates (Figure S8c), where nanosheets completely disappearing. Instead, ultrafine nanocrystals tend to spontaneously together forming 3D spherical structures (Figure S8d) rather than arranging in 2D planar direction. So the current experiments demonstrate that directional hydrophobic attraction plays a crucial role in determining morphologies of final products. The formation of ultrathin nanosheets in our microwave-assisted liquid-phase growth procedure is attributed to two factors: layered-structural nature and hydrophobicity. It is well known that the 2D anisotropic growth of nanomaterials needs larger driving force. In case of the layered crystals, they have the tendency to growth into layers. So the intrinsic driving force of lamellar nickel hydroxide is adequate for their 2D anisotropic growth under microwave activation. The layered-structural nature is believed to be a prerequisite for the formation of 2D network in the present facile method. The required hydrophobicity can bring about directional hydrophobic attraction between nanocrystals and water molecules, forming two-phase interfaces where the excessive surface energy can be accommodated. A balance of anisotropic hydrophobic attraction and electrostatic interaction can be realized, which is favorable for the spontaneous organization of nanocrystals into nanosheets[27,28]. The resulted interaction could allow for the epitaxial orientation of ultrafine nanocrystals and hinder their potential of shrinking and aggregating. Furthermore, the presence of the hydrophobicity could also terminate their stacking and packing, leading to ultrathin 2D structure rather than 3D graphite-like layered framework.

To investigate local atomic arrangements and electronic structures of ultrathin α-$Ni(OH)_2$ nanosheets, X-ray absorption fine structure spectroscopy (XAFS) measurements at Ni K-edge are conducted. Figure 4a shows the typical layered structure model. Figure 3b shows that the observed spectral peaks for α-$Ni(OH)_2$ nanosheets slightly shift to the higher energy direction. Particularly, the most remarkable difference appears in the main peak locating at around 8351 eV in terms of position and intensity. This result evidently manifests the affection of interlayer scattering toward the observed spectrum. The ultrathin thickness (1.52 nm) means the few layers (2–3) of the α-$Ni(OH)_2$ nanosheets, which deliver a little interlayer scattering. The removing of interlayer scattering causes the shift of the three major peaks to the higher energy side[29]. Ni K-EXAFS $k^2x(k)$ oscillation curve for nanosheets (Figure 3c) exhibits a small reduction in amplitude and a little difference in spectral shape compared with that of bulk counterpart, implying the different local atomic arrangement. The nanosheets exhibit three obvious differences in Fourier transform curve (Figure 3d). First, the Ni-O2/O3 peak intensity of the nanosheets decreases significantly to noise level, which can be attributed to the missing contribution from the O3 atoms. This result once again demonstrates the few layer structure of the ultrathin nanosheets. Secondly, the nanosheets show a shift toward a shorter distance and an intensity decrease in the Ni-Ni3 peak. The shift can be attributed to the presence of surface structure distortion on nanosheets. While the particularly strong Ni-Ni3 peak for the bulk mainly caused by the focusing effect from the Ni1 atom situated halfway on the Ni-Ni3 path[29]. Thirdly, the Ni-Ni1 peak for the nanosheets slightly shifts toward a shorter distance. But the Ni-O1 peak shows no shift with intensity similar to the corresponding bulk peak. These facts suggest that the structural contraction occurs parallel to the Ni layer (i.e. along the *ab* plane) in nanosheets, which also means a noticeable distortion on surface of the nanosheets that in turn helps to balance their excessive surface energy and then allow them with excellent stability[11].

Ultrathin 2D nanomaterials represent a great promising application in next generation batteries and supercapacitors. With respect to the ultrathin α-$Ni(OH)_2$ and NiO nanosheets, which are almost completely made up by surfaces with the most active material exposed outside for the highly surface-dependent Faradaic redox reactions, their potential in supercapacitor are systematically investigated. Figure 4 shows typical Cyclic voltammogram (CV) curves of the ultrathin α-$Ni(OH)_2$ nanosheets. A pair of current peaks can be clearly observed during the cathodic and anodic sweeps, which correspond to the reversible conversion between Ni(II) and Ni(III)[30–32].

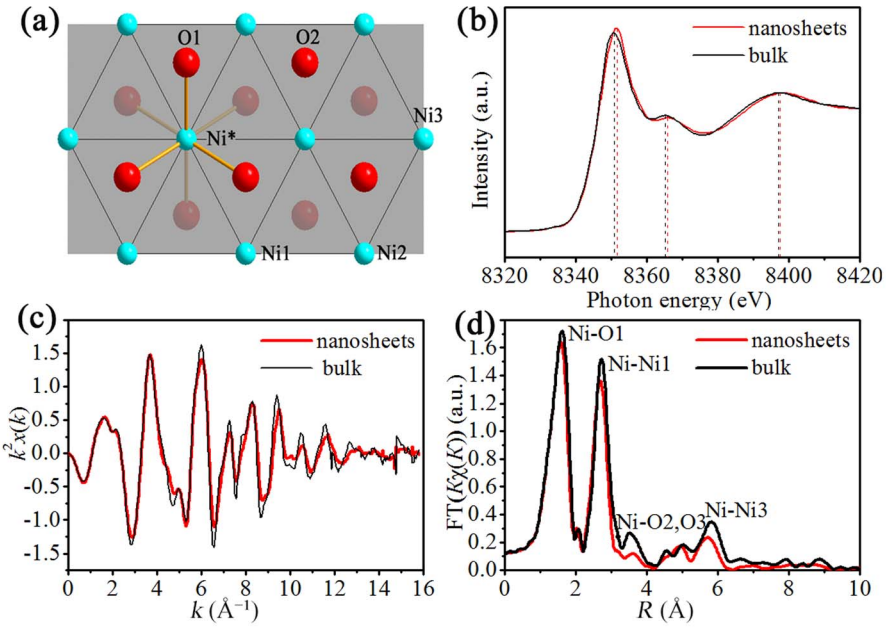

Figure 3 | (a) Schematic structure model of α-$Ni(OH)_2$ single layer along c axis. The shadow represents the (001) plane. The third-nearest neighbor oxygen atom (O3) is situated in the adjacent layer (not shown); (b) Ni K-edge XANES spectra of the α-$Ni(OH)_2$ nanosheets and their bulk counterpart; (c) Ni K-EXAFS oscillation functions $k^2x(k)$ and (d) the corresponding Fourier transforms.

The reaction involves the reversible process of insertion and extraction of OH^{-1} ions. This result reveals that the charge storage mechanism of the α-$Ni(OH)_2$ nanosheet electrodes is mainly ascribed to the pseudocapacitance from the Faradaic processes. Furthermore, the redox peaks show a symmetric characteristic, suggesting a high reversibility of α-$Ni(OH)_2$ nanosheets. Apparently, the current density increases with the increasing scan rate, and all CV curve maintain a similar shape, indicating that the ultrathin α-$Ni(OH)_2$ nanosheets are beneficial to fast redox reactions. The CV curves show more prominent symmetry at higher scan rates indicating better high-rate response of the α-$Ni(OH)_2$ nanosheets. In addition, as the scan rate increased, the potential of the anodic and cathodic peaks shifted in more positive and negative directions, respectively, most likely attributed to a high electron hopping resistance or the limitation of the ion diffusion rate to satisfy electronic neutralization during the redox reaction.

As shown in Figure 5a, all the nonlinear discharge curves confirm the pseudocapacitive characteristic. Encouragingly, the ultrathin

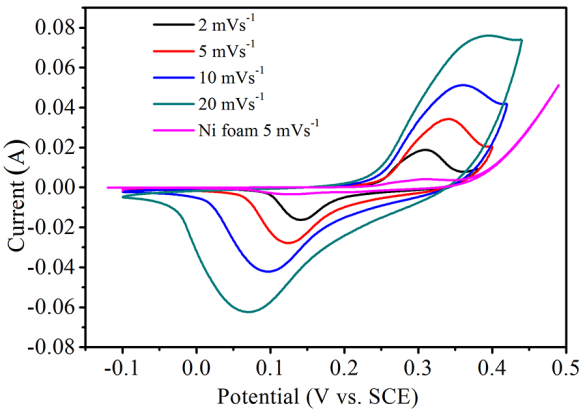

Figure 4 | **Typical CV curves of α-$Ni(OH)_2$ nanosheets at different scan rates in 6 M KOH electrolyte.** The CV curve for the pristine Ni foam current collector at 5 mV s^{-1} is also listed for comparison demonstrating a negligible CV background.

α-$Ni(OH)_2$ nanosheets deliver a ultrahigh specific capacitance of 4172.5 F g^{-1} at 1 A g^{-1} (Figure 5b). This specific capacitance is the highest value reported up to now. The ever reported high specific capacitance is 3500 F g^{-1} for $Co(OH)_2$ on ultra-stable Y zeolite[33], but still lower than our current result. As the discharge current density increased, the ultrahigh specific capacitance is still maintained. The specific capacitances are 3650, 3270, 2820, and 2680 F g^{-1} at 2, 4, 8, and 16 A g^{-1}, respectively. The specific capacitance gradually decreases at higher current density due to the incremental (iR) voltage drop. It is found that all the obtained specific capacitances are higher than the corresponding results in previous reports respectively checked at the same current density. It is well known that fabricating direct nanostructured electrodes is the most attractive strategy, such as highly ordered nanostructured array electrode, to achieve ultrahigh electrochemical performances. For example, Yang reported electrodeposited $Ni(OH)_2$ on nickel foam as direct nanostructured electrodes and obtained a high specific capacitance of 3152 F g−1 at 4 A g^{-1} current density[34], yet slightly lower than our 3270 F g^{-1}; Yuan fabricated the Ni foam supported ultrathin mesoporous $NiCo_2O_4$ nanosheets electrodes achieving excellent pseudocapacitance of 1694 F g^{-1} at 8 A g^{-1} current density[35]; Shang reported the coaxial $Ni_xCo_{2x}(OH)_{6x}$/TiN nanotube arrays as supercapacitor electrodes, exhibiting a high specific capacitance of 2543 F g^{-1} calculated from the CV curves (5 mV s^{-1})[36]. In practice, using of direct nanostructured electrodes is favorable for proof-concept studies or for microdevices, but unlikely for commercial applications, especially in electric vehicles or power grid storage. Remarkably, the specific capacitances of our α-$Ni(OH)_2$ nanosheets are distinctly superior to that of the conceptual designing direct nanostructured electrodes.

when current density is increased to 16 A g^{-1}, the specific capacitance is still 2680 F g^{-1}, and retain 64.2% of its initial value with a current density increase of 16 times, indicating excellent rate capability due to short diffusion path distances. The specific capacitances are larger than the theoretical value of 2602 F g^{-1} (within 0.4 V). Besides pseudocapacitance derived from the Faradaic redox reactions, contributions from double-layer capacitance are obvious. Considering the high specific surface area from α-$Ni(OH)_2$ nanosheets, contribution from double-layer capacitance certainly supply

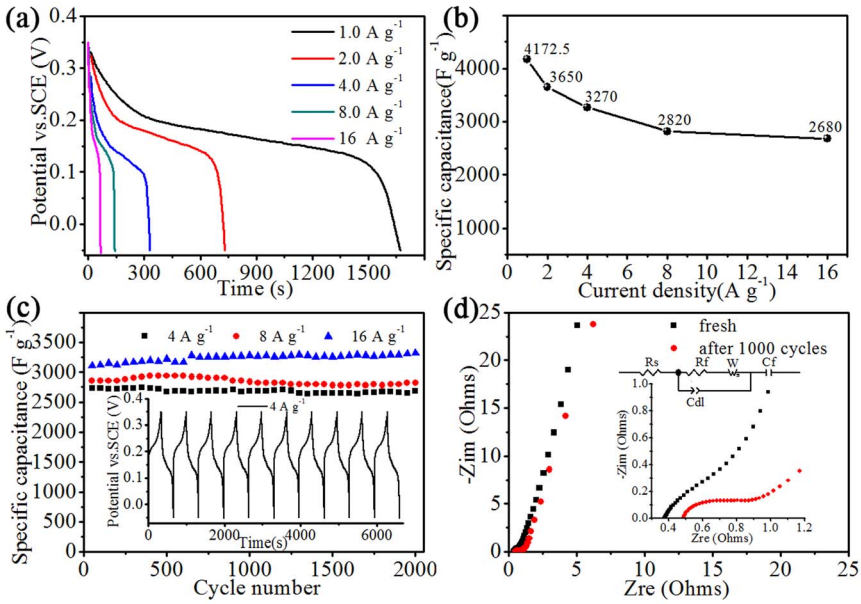

Figure 5 | Electrochemical characterization of α-Ni(OH)$_2$ nanosheets: (a) discharge curves; (b) specific capacitance as a function of current densities; (c) average specific capacitance versus cycle number, the inset shows the galvanostatic charge-discharge curves at current density of 4 A g^{-1}; (d) Nyquist plots before and after cycling at current density of 4 A g^{-1}, (inset) equivalent fitting circuit and impedance at high frequency region.

an additional boost to the observed value. As shown in Figure 5c, the α-Ni(OH)$_2$ nanosheets exhibit excellent cycling stability. The average specific capacitance at 4 A g^{-1} increases gradually up to 3320 F g^{-1} in the course of 2000 cycles with a high capacitance retention of 101.5%, due to full activation of electrode material. Even at high rates, 8 and 16 A g^{-1}, the capacitance retention after 2000 cycles is still maintained at 100% and 98.5%, respectively, indicating stable cycling performance at each current density. The insert in Figure 5c further indicates that the fast charge-discharge process of the electrode is highly reversible.

The good electrochemical reversibility and high rate capability can be further explained by EIS measurements (Figure 5d). The Nyquist spectrum can be well represented by an equivalent circuit as the insert shown. The first intersecting point with the real axis in the high-frequency region represents the internal resistance (Rs) including ionic resistance of electrolyte, inherent resistance of active material, and contact resistance at the interface of active material-current collector[37,38]. Throughout experiments, the current collector and the α-Ni(OH)$_2$ nanosheets are well attached together, except a slightly increased Rs. The Rs are evaluated to be approximately 0.37 and 0.49 Ω, respectively, before and after 1000 cycles. The slightly increased Rs is mainly attributed to the contact resistance due to the fact that the repetitive insertion and extraction of OH^{-1} ions lead to active material partially disconnecting from current collector. The high frequency semicircle is attributed to the charge-transfer process of Faradic reactions occurring at the electrode-electrolyte interface. The semicircle diameter reflects charge-transfer resistance (Rf)[39]. After 1000 cycles, the Rf is not significantly altered, indicative of the best electrical conductivity and activity. The α-Ni(OH)$_2$ nanosheets show nearly vertical Warburg slope in both Nyquist spectrum of the initial one and the 1000th cycle, no significant variation is observed. This result suggests that the Warburg resistance has no determinable affect for the electrode to store charges more efficiently.

Discussion

Based on the liquid-phase growth of lamellar hydroxide precursors, it could summarize an intermediate strategy assisted by microwave irradiation for large-scale synthesis of ultrathin 2D nanosheets of non-layered transition metal oxides for the first time. The combination with microwave heating makes it time-saving. The present procedure requires only simple reagents and equipment, carried out under moderate conditions. In the initial growth stage, the main reaction is conducted in an open system rather than in any high-pressure vessels, without seeding protocols or ultrafine control over the temperature and pressure. The weight of the final α-Ni(OH)$_2$ and NiO nanosheets are 1.48 and 1.14 g at one time synthesis (Figure S1b–c). The process is easily scaled up and the approach can lead to ultrathin 2D nanosheets in high yield, demonstrating it very cost-effective and greatly competitive for industrialized production of high-quality ultrathin 2D nanosheets.

The ultrathin NiO nanosheets also delivered a high specific capacitance of 2236 F g^{-1} at 0.5 A g^{-1} (Figure S9). Even at higher current densities, the specific capacitance is still maintained at 1392 F g^{-1} at 12 A g^{-1}, and 1576 F g^{-1} at 4 A g^{-1} with 99.1% retention after 2000 cycles, suggesting good rate capability and excellent cycling stability(analysis in detail see Supporting Information). The excellent properties must be associated with fast and efficient ion pathways derived from of the ultrathin structure with a large surface area. In the desirable architecture, a maximum active material utilization and favorable reaction kinetics are guaranteed. Consequently, surface-enhanced performances are achieved by combining short diffusion distances, large electrochemical active surface area of those ultrathin nanosheets.

In summary, we have developed a facial method for large-scale synthesis of high-quality ultrathin 2D nanosheets of hydroxides and transition metal oxides. The nanosheet formation in liquid-phase is attributed to two factors: layered-structural nature and hydrophobicity. The nanosheets exhibit a large planar area and ultrathin thickness. Their special surface properties can facilitate the surface-dependent electrochemical reaction processes. The ultrathin α-Ni(OH)$_2$ and NiO nanosheets exhibit high specific capacitance as well as good rate capability and excellent cycling stability. This work provides an innovation in fabricating ultrathin 2D nanomaterials and extension to non-layered compound as well as the potential of advanced electrodes for next-generation electrochemical energy storage devices.

Methods

Materials synthesis and characterization. The chemical reagents were of analytical grade and used as received. The α-$Ni(OH)_2$ nanosheets were synthesized through a facile and scalable microwave-assisted method. Briefly, certain amounts of nickel (II) nitrate hexahydrate and urea with molar ratio of 1 : 4 were dissolved in 30 mL deionized water, and then 210 mL ethylene glycol was added in, forming a homogeneous solution. The resulting solution was transferred into a 1000 mL homemade round-bottomed flask and treated under microwave irradiation in a SINEO MAS-II microwave reactor (Figure S1a) at 700 W for several minutes. Finally, puffy grass-green colloid precipitates were obtained, and then cooled down to room temperature naturally. After retrieved by centrifugation and washed several times with distilled water and absolute ethanol, the resulting green product was dried in vacuum at 80°C for 12 h. The final NiO nanosheets were obtained through heat treatment of the nickel hydroxide precursor at 300°C for 2 h.

Characterizations of the samples were carried out by X-ray diffractometry (XRD; Bruker D8, CuKa source), field emission scanning electron microscopy (FESEM, Hitachi S-4800) equipped with energy-dispersive X-ray spectroscopy (EDS, Oxford Instruments, INCA), and transmission electron microscopy (TEM, JSM-2100F, 200 kV), and high-resolution TEM (HRTEM, FEI Tecnai G2 F20, 200 kV).The Brunauer-Emmett-Teller specific surface areas (BET) and porosity of the samples were evaluated on the basis of nitrogen adsorption isotherms using a NOVA4200e nitrogen adsorption apparatus (Quantachrome Instruments, USA). Thermogravimetrics (TGA) analysis was carried out by ZRY-2P thermal analysis equipment in air atmosphere with 10°C min^{-1}. X-ray photoelectron sperctra (XPS) were recorded on a PHI Quanteral II (Japan) with an Al K = 280.00 eV excitation source. The binding energies were calibrated by referencing the C1s peak to reduce the sample charge effect. The Ni K-edge XAFS were measured at the 1W1B beamline of the Beijing Synchrotron Radiation Facility (BSRF, China). The storage ring energy was operated at 2.5 GeV with a maximum current 250 mA in the decay mode. A Si (111) double crystal was used as the monochromator. Data were collected in transmission mode with ionization chambers filled with a N_2/Ar mixture at room temperature. The energy calibration was performed with a Ni foil at 8333 eV. In the energy range selected for the experiments a detuning of 30% between silicon crystals was performed to suppress the high harmonic content. Fine samples were brushed onto Kapton tapes that were stacked together to give approximately one x-ray-absorption length at the Ni K-edge, following the traditional sample prepared method[40,41]. Data processing and analysis were made by standard procedures[42].

Electrochemical measurements. The procedures of making electrodes and measurements could be found elsewhere[43]. In practice, The working electrodes were fabricated by mixing the as-prepared active material, acetylene black, and poly(tetrafluoroethylene) (PTFE) in a mass ratio of 75 : 15 : 10 with ethanol, then sonicated for 30 minutes to form a homogeneous slurry. Then the resulting mixture was coated on the pretreated battery-grade nickel foam (0.2 mm thick). The mass variation was reduced using a constant volume of slurries by microinjector (loading mass 1 ± 0.03 mg), and dried at 90°C for 12 h in a vacuum oven. The nickel foam with active materials were finally pressed under 10 MPa for 30 seconds to obtain the working electrode. The exposed geometric area of these electrodes is equal to 1 cm^2 and the other surface areas were coated with epoxy resin adhesive. Electrochemical measurements were carried out using a three-electrode system. The 6 M and 2 M KOH solution were used as electrolyte for α-$Ni(OH)_2$ and NiO nanosheets, respectively. A platinum foil (1 × 2 cm^2), and a saturated calomel electrode (SCE) were used as counter electrode and reference electrode, respectively. The cyclic voltammogram (CV) and electrochemical impedance spectroscopy (EIS) were measured on CHI660C electrochemical workstation (Shanghai Chenhua Co. Ltd., China) and IM6e electrochemical workstation (Zahner, Germany). CV tests of α-$Ni(OH)_2$ nanosheet electrode were carried out between −0.1 and 0.43 V (vs. SCE) at various scan rates, respectively, and the EIS measurements were collected in the frequency range from 0.01 Hz to 100 kHz at open-circuit potential of ~0.23 V with an alternating current (ac) amplitude of 5 mV. Galvanostatic charge/discharge curves of α-$Ni(OH)_2$ and NiO nanosheets were measured in the potential range of −0.05 to 0.35 V and −0.05 to 0.45 V at different current densities on a CT2001A LAND Cell test system.

1. Wang, H., Casalongue, H. S., Liang, Y. & Dai, H. $Ni(OH)_2$ nanoplates grown on graphene as advanced electrochemical pseudocapacitor materials. *J. Am. Chem. Soc.* **132**, 7472–477 (2010).
2. Ji, J. *et al.* Nanoporous $Ni(OH)_2$ thin film on 3D ultrathin-graphite foam for asymmetric supercapacitor. *ACS Nano* **7**, 6237–6243 (2013).
3. Yu, Z., Duong, B., Abbitt, D. & Thomas, J. Highly ordered MnO_2 nanopillars for enhanced supercapacitor performance. *Adv. Mater.* **25**, 3302–3306 (2013).
4. Cao, C. Y., Guo, W., Cui, Z. M., Song, W. G. & Cai, W. Microwave-assisted gas/liquid interfacial synthesis of flowerlike NiO hollow nanosphere precursors and their application as supercapacitor electrodes. *J. Mater. Chem.* **21**, 3204–3209 (2011).
5. Ding, S., Zhu, T., Chen, J. S., Wang, Z., Yuan, C. & Lou, X. W. Controlled synthesis of hierarchical NiO nanosheet hollow spheres with enhanced supercapacitive performance. *J. Mater. Chem.* **21**, 6602–6606 (2011).
6. Sun, X., Wang, G., Hwang, J. Y. & Lian, J. Porous nickel oxide nano-sheets for high performance pseudocapacitance materials. *J. Mater. Chem.* **21**, 16581–16588 (2011).
7. Meher, S. K., Rao, G. R., Meher, S. K. & Rao, G. R. Ultralayered Co_3O_4 for high-performance supercapacitor applications. *J. Phys. Chem. C* **115**, 15646–15654 (2011).
8. Wang, X., Feng, H., Wu, Y. & Jiao, L. Controlled synthesis of highly crystalline MoS_2 flakes by chemical vapor deposition. *J. Am. Chem. Soc.* **135**, 5304–5307 (2013).
9. Feng, J. *et al.* Metallic few-layered VS_2 ultrathin nanosheets: high two-dimensional conductivity for in-plane supercapacitors. *J. Am. Chem. Soc.* **133**, 17832–17838 (2011).
10. Du, Y. *et al.* A general method for the large-scale synthesis of uniform ultrathin metal sulphide nanocrystals. *Nat. Commun.* **3**, 1177 (2012).
11. Sun, Y. *et al.* Fabrication of flexible and freestanding zinc chalcogenide single layers. *Nat. Commun.* **3**, 1057 (2012).
12. Wang, G. *et al.* Sn/graphene nanocomposite with 3D architecture for enhanced reversible lithium storage in lithium ion batteries. *J. Mater. Chem.* **19**, 8378–8384 (2009).
13. Takagaki, A., Tagusagawa, C., Hayashi, S., Hara, M. & Domen, K. Nanosheets as highly active solid acid catalysts for green chemical syntheses. *Energy Environ. Sci.* **3**, 82–93 (2010).
14. Liu, J. & Liu, X. W. Two–dimensional nanoarchitectures for lithium storage. *Adv. Mater.* **24**, 4097–4111 (2012).
15. Guo, S. & Dong, S. Graphene nanosheet: synthesis, molecular engineering, thin film, hybrids, and energy and analytical applications. *Chem. Soc. Rev.* **40**, 2644–2672 (2011).
16. Rangappa, D., Murukanahally, K. D., Tomai, T., Unemoto, A. & Honma, I. Ultrathin nanosheets of Li_2MSiO_4 (M = Fe, Mn) as high-capacity Li-ion battery electrode. *Nano Lett.* **12**, 1146–1151 (2012).
17. Liu, J., Chen, J. S., Wei, X., Lou, X. W. & Liu, X. W. Sandwich–Like, stacked ultrathin titanate nanosheets for ultrafast lithium storage. *Adv. Mater.* **23**, 998–1002 (2011).
18. Zhu, Y. *et al.* Carbon–based supercapacitors produced by activation of graphene. *Science* **332**, 1537–1541 (2011).
19. Son, J. S. *et al.* Large–scale soft colloidal template synthesis of 1.4 nm thick CdSe nanosheets. *Angew. Chem.* **121**, 6993–6996 (2009).
20. Vaughn II, D. D., Patel, R. J., Hickner, M. A. & Schaak, R. E. Single–crystal colloidal nanosheets of GeS and GeSe. *J. Am. Chem. Soc.* **132**, 15170–15172 (2010).
21. Schliehe, C. *et al.* Ultrathin PbS sheets by two-dimensional oriented attachment. *Science* **329**, 550–553 (2012).
22. Yu, T., Lim, B. & Xia, Y. Aqueous–phase synthesis of single–crystal ceria nanosheets. T. Yu, B. Lim, Y. Xia. *Angew. Chem. Int. Ed.* **49**, 4484–4487 (2010).
23. Frindt, R. F. Single crystals of MoS_2 several molecular layers thick. *J. Appl. Phys.* **37**, 1928–1929 (1966).
24. Baghbanzadeh, M., Carbone, L., Cozzoli, P. D. & Kappe, C. O. Microwave–assisted synthesis of colloidal inorganic nanocrystals. *Angew. Chem. Int. Ed.* **50**, 11312–11359 (2011).
25. Bilecka, I. & Niederberger, M. Microwave chemistry for inorganic nanomaterials synthesis. *Nanoscale* **2**, 1358–1374 (2010).
26. Gou, L., Chipara, M. & Zaleski, J. M. Convenient, rapid synthesis of Ag nanowires. *Chem. Mater.* **19**, 1755–1760 (2007).
27. Tang, Z., Zhang, Z., Wang, Y., Glotzer, S. C. & Kotov, N. A. Self-assembly of CdTe nanocrystals into free-floating sheets. *Science* **314**, 274–278 (2006).
28. Zhang, Z., Tang, Z., Kotov, N. A. S. & Glotzer, C. Simulations and analysis of self-assembly of CdTe nanoparticles into wires and sheets. *Nano Lett.* **7**, 1670–1675 (2007).
29. Ichiyanagi, Y. *et al.* X-ray absorption fine-structure study on the $Ni(OH)_2$ monolayer nanoclusters. *Chem. Phys. Lett.* **379**, 345–350 (2003).
30. Tang, Z., Tang, C. & Gong, H. A high energy density asymmetric supercapacitor from nano-architectured $Ni(OH)_2$/carbon nanotube electrodes. *Adv. Funct. Mater.* **22**, 1272–1278 (2012).
31. Liu, J., Cheng, C., Zhou, W., Li, H. & Fan, H. J. Ultrathin nickel hydroxidenitrate nanoflakes branched on nanowire arrays for high-rate pseudocapacitive energy storage. *Chem. Commun.* **47**, 3436–3438 (2011).
32. Zhang, H. *et al.* One-step electrophoretic deposition of reduced graphene oxide and $Ni(OH)_2$ composite films for controlled syntheses supercapacitor electrodes. *J. Phys. Chem. B* **117**, 1616–1627 (2013).
33. Cao, L., Xu, F., Liang, Y. Y. & Li, H. L. Preparation of the novel nanocomposite $Co(OH)_2$/ultra-stable Y zeolite and its application as a supercapacitor with high energy density. *Adv. Mater.* **16**, 1853–1857 (2004).
34. Yang, G. W., Xu, C. L. & Li, H. L. Electrodeposited nickel hydroxide on nickel foam with ultrahigh capacitance. *Chem. Commun.* **48**, 6537–6539 (2008).
35. Yuan, C., Li, J., Hou, L., Zhang, X., Shen, L. & Lou, X. W. Ultrathin mesoporous $NiCo_2O_4$ nanosheets supported on Ni foam as advanced electrodes for supercapacitors. *Adv. Funct. Mater.* **22**, 4592–4597 (2012).
36. Shang, C. *et al.* Coaxial $Ni_xCo_{2x}(OH)_{6x}$/TiN nanotube arrays as supercapacitor electrodes. *ACS Nano* **7**, 5430–5436 (2013).
37. Li, X., Rong, J. & Wei, B. Electrochemical behavior of single-walled carbon nanotube supercapacitors under compressive stress. *ACS Nano* **4**, 6039–6049 (2010).
38. Li, X., Gu, T. & Wei, B. Dynamic and galvanic stability of stretchable supercapacitors. *Nano Lett.* **12**, 6366–6371 (2012).

39. Zhou, C., Zhang, Y., Li, Y. & Liu, J. Construction of high-capacitance 3D CoO@ Polypyrrole nanowire array electrode for aqueous asymmetric supercapacitor. *Nano Lett.* **13**, 2078–2085 (2013).
40. Wu, Z. Y. *et al.* Quadrupolar transitions and medium-range-order effects in metal K-edge x-ray absorption spectra of 3d transition-metal compounds. *Phys. Rev. B*, **70**, 033104 (2004).
41. Chu, W. *et al.* Iron isotope effect and local lattice dynamics in the (Ba, K)Fe_2As_2 superconductor studied by temperature-dependent EXAFS. *Sci. Rep.* **3**, 1750 (2013).
42. Ravel, B. & Newville, M. ATHENA, ARTEMIS, HEPHAESTUS: data analysis for X-ray absorption spectroscopy using IFEFFIT. *J. Synchrotron Rad.* **12**, 537–541 (2005).
43. Xiao, Y. *et al.* 3D Hierarchical Co_3O_4 twin-spheres with an urchin-like structure: large-scale synthesis, multistep-splitting growth, and electrochemical pseudocapacitors. *Adv. Funct. Mater.* **22**, 4052–4059 (2012).

Acknowledgments

We gratefully thank the National Natural Science Foundation of China (No. 21371023, Creative Research Groups 11321503) and the Knowledge Innovation Program of the Chinese Academy of Sciences (KJCX2-YW-N42).

Author contributions

Y.Z. explored the strategy for fabricating the samples and carried out experiment. C.C. and Y.L. designed the research approach and provided guidance. S.T., W.C. and Z.W. collected and analyzed the XAFS data. Y.Z. and C.C. wrote the manuscript and all authors discussed the experiments and final manuscript.

Additional information

Supplementary information accompanies this paper at http://www.nature.com/scientificreports

Competing financial interests: The authors declare no competing financial interests.

How to cite this article: Zhu, Y.Q. *et al.* Ultrathin Nickel Hydroxide and Oxide Nanosheets: Synthesis, Characterizations and Excellent Supercapacitor Performances. *Sci. Rep.* **4**, 5787; DOI:10.1038/srep05787 (2014).